A Density Functional Study of EPR Parameters for Vanadyl Complexes Containing Schiff Base Ligands

Markéta L. Munzarová[†,‡] and Martin Kaupp*[,‡]

National Center for Biomolecular Research, Faculty of Science, Masaryk University, Kotlávská 2, CZ-61137 Brno, Czech Republic, and Institut für Anorganische Chemie, Universität Würzburg, Am Hubland, D-97074 Würzburg, Germany

Received: July 12, 2001; In Final Form: October 5, 2001

Deviations of the coordination arrangement of vanadyl complexes from a regular square pyramid are thought to influence, among other things, their biological function. Such structural distortions have been found to be reflected characteristically in EPR spectra (Cornman et al. *Inorg. Chem.* **1997**, *3*66, 6401). In this work, density functional calculations of electronic *g* tensors and metal hyperfine coupling tensors have been carried out for a series of four of these vanadyl complexes with structures ranging from nearly trigonal bipyramidal (TBP-5) to nearly square pyramidal (SQP-5). The EPR spectroscopic parameters have been rationalized in terms of electronic and geometrical structures. Using all relevant perturbation operators together with local or gradient-corrected density functionals, Δg-tensor components are underestimated systematically by ca. 40%. Good agreement with experiment is obtained for hyperfine tensor components calculated with hybrid functionals (B3PW91 and BHPW91), which account better for the spin polarization of the core orbitals than GGA functionals such as BP86. The rhombicity of the hyperfine tensor is reproduced well at all levels of theory applied. It is mainly determined by the SOMO composition. The latter explains the increasing rhombicity of the *A* tensor with increasing distortion of the SQP-5 structures along the series of complexes studied. The orientational dependence of the principal tensor components on the local vanadium coordination is much more pronounced for the *g* tensor than for the *A* tensor. The principal axes of the *g* and *A* tensors are found to be rotated with respect to each other by as much as 41°.

1. Introduction

The coordination chemistry of vanadium has recently received increased attention, because of the discovery of enzymes requiring vanadium for activity[1] and because of the insulin-like effects elicited by vanadium complexes in diabetic animals.[2] The biochemical activity of vanadium is often related to the interplay between four-coordinate tetrahedral structures of vanadates(V) and five-coordinate trigonal bipyramidal (TBP-5) structures of vanadyl(IV) or vanadyl(V) complexes.[3] The TBP-5 coordination appears to be the consequence of significant steric constraints, as square pyramidal (SQP-5) or distorted SQP-5 complexes are formed in the absence of bulky ligands.[4] To probe these constraints, Cornman et al. have recently prepared a series of vanadyl complexes, in which the coordination arrangement varied from approximately SQP-5 to approximately TBP-5.[5] An angular structural parameter τ (ranging from $\tau = 0$ for purely SQP-5 coordination to $\tau = 1$ for purely TBP-5 coordination) has been introduced to quantitatively compare the coordination sphere of the metal. The value of τ varied from 0.26 to 0.70 for the complexes studied in ref 5. EPR and pulsed ENDOR studies showed that both hyperfine coupling (HFC) tensor components and nuclear quadrupole coupling constant $P_{||}$ provide a sensitive measure of changes in the arrangement of the ligands.[5−7] In particular, it was noted[5] that the EPR spectra of all complexes are rhombic and that the rhombicity increases with τ.

Our previous systematic applications of density functional theory (DFT) to the calculation of hyperfine tensors in a series of 3d transition metal complexes have taught us that explicit quantum chemical studies may provide considerably refined interpretations of the observed spectroscopic parameters.[8,9] A recently developed DFT approach[10] for the calculation of electronic *g* tensors allows us furthermore to extend our computational investigations also to this property. Here, we report a detailed DFT study of hyperfine coupling and *g* tensors for some of the complexes studied by Cornman et al.[5] and for bis(2-methylquinoline-8-olate)oxovanadium(IV). For the latter complex, single-crystal EPR studies have provided magnitudes, as well as absolute and relative orientations, of the hyperfine and *g* tensors.[11] We will relate the experimental and computational findings to the distribution of spin density within the complexes studied and will provide an interpretation of the correlation between the rhombicity of the tensors and τ.

2. Theoretical Formalism and Computational Details

***g*-Tensor Calculations.** The theoretical background of EPR parameters is covered in detail in text books.[12−17] Hence we summarize only the most relevant points and the expressions used in our calculations. The *g* tensor is calculated as a correction to the free electron value (given in ppt), i.e.

$$\mathbf{g} = g_e\mathbf{1} + \Delta\mathbf{g} \qquad (1)$$

with $g_e = 2.002319$. Up to the level of second-order perturbation theory, the g shift $\Delta\mathbf{g}$ consists of the relevant Breit−Pauli terms

* To whom correspondence should be addressed. E-mail: kaupp@mail.uni-wuerzburg.de.
† Masaryk University.
‡ Universität Würzburg.

10.1021/jp015506y CCC: $20.00
Published on Web 11/17/2001

$$\Delta\mathbf{g} = \Delta\mathbf{g}_{SO/OZ} + \Delta\mathbf{g}_{RMC} + \Delta\mathbf{g}_{GC} \quad (2)$$

of which the "paramagnetic" second-order spin−orbit/orbital Zeeman cross term, $\Delta\mathbf{g}_{SO/OZ}$, dominates (except for extremely small Δg values; we also include $\Delta\mathbf{g}_{RMC}$ and the $\Delta\mathbf{g}_{GC}$(1el.) in the calculations[10]). Within the present uncoupled DFT (UDFT) approach, its Cartesian components u,v are computed as[10,18]

$$\Delta\mathbf{g}_{SO/OZ,uv} = \frac{\alpha^2}{2} g_e \left[\sum_k^{occ(\alpha)} \sum_a^{virt(\alpha)} \frac{\langle\psi_k^\alpha|H_{SO,v}|\psi_a^\alpha\rangle\langle\psi_a^\alpha|l_{O,u}|\psi_k^\alpha\rangle}{\epsilon_k^\alpha - \epsilon_a^\alpha} - \sum_k^{occ(\beta)} \sum_a^{virt(\beta)} \frac{\langle\psi_k^\beta|H_{SO,v}|\psi_a^\beta\rangle\langle\psi_a^\beta|l_{O,u}|\psi_k^\beta\rangle}{\epsilon_k^\beta - \epsilon_a^\beta} \right] \quad (3)$$

We calculate the spin−orbit (SO) operator H_{SO} in the atomic mean-field approximation (AMFI).[19,20] This approach has been shown[10] to give results to within better than a few percent of the exact Breit−Pauli one- and two-electron SO Hamiltonian, at a small fraction of the computational effort required for the latter. For comparison, we also report results in which the two-electron spin−orbit contributions have been neglected, and only the one-electron part due to the nuclear charges has been retained. We employed a common gauge at the transition metal nucleus. Unrestricted Kohn−Sham calculations were performed within the local density approximation (VWN functional).[21] Gradient corrected functionals do not improve the results in the case of g tensors of transition metal complexes.[10] The (15s11p6d)/[9s7p4d] metal basis set employed in our previous studies[8−10] has been used. DZVP basis sets[22] were used for the main group atoms. Polarization p functions have been omitted for hydrogens of the methyl and *t*-butyl substituents. The g tensor results for VOL^1, $VO(L^2)_2$, and $VO(L^3)_2$, at the UDFT-VWN level, have already been included in our previous systematic validation study of the g tensor code. However, in that work, neither tensor orientations nor the relations between electronic structure and g tensor had been discussed.[10]

Hyperfine Tensor Calculations. The hyperfine coupling parameters describe the interactions of unpaired electrons with various magnetic nuclei. The 3×3 hyperfine interaction tensor A can be separated into its isotropic and anisotropic (dipolar) components. The isotropic part reflects the spin density at the point of the magnetic nucleus. The anisotropic part yields additional information about the local environment of a paramagnetic center. In the first-order approximation (neglecting spin−orbit effects; cf. below), isotropic hyperfine splittings $A_{iso}(N)$ correspond to the Fermi-contact term A_{FC}:

$$A_{iso}(N) = A_{FC} = \frac{4\pi}{3}\beta_e\beta_N g_e g_N \langle S_Z\rangle^{-1} \sum_{\mu,\nu} P_{\mu,\nu}^{\alpha-\beta} \langle\varphi_\mu|\delta(R_N)|\varphi_v\rangle \quad (4)$$

Here, β_e is the Bohr magneton, β_N is the nuclear magneton, g_N is the g value of the nucleus N, $\langle S_Z\rangle$ is the expectation value of the z component of the total electronic spin, $P_{\mu,\nu}^{\alpha-\beta}$ is the spin density matrix, and summation runs over all occupied molecular orbitals. In the first-order approximation, the components T_{ij} of the anisotropic tensor are given by

$$T_{ij}(N) = \frac{1}{2}\beta_e\beta_N g_e g_N \langle S_Z\rangle^{-1} \sum_{\mu,\nu} P_{\mu,\nu}^{a-\beta} \langle\varphi_\mu|\mathbf{r}_N^{-5}(\mathbf{r}_N^2\delta_{ij} - 3r_{N,i}r_{N,j})|\varphi_\nu\rangle \quad (5)$$

where $\boldsymbol{r}_N = \boldsymbol{r} - \boldsymbol{R}_N$ ($\boldsymbol{R}_N$ is the position vector of nucleus N). In the following, we will generally refer to the metal hyperfine interaction, and argument N will be omitted.

All-electron unrestricted Kohn−Sham calculations of hyperfine structure were done with the Gaussian 98 program.[23] We have used three different combinations of exchange and correlation potentials ($\nu_x[\rho]$ and $\nu_c[\rho]$, respectively), abbreviated as BP86, B3PW91, and BHPW91. The BP86 functional combines Becke's generalized gradient correction (GGA) functional for exchange[24] (B) with Perdew's 1986 GGA[25] (P86) for correlation. B3PW91 contains Becke's three-parameter hybrid functional for exchange (B3, including ca. 20% Hartree−Fock exchange),[26] whereas the last combination employs the "half-and-half" hybrid exchange functional (BH), incorporating as much as 50% Hartree−Fock exchange.[27] The latter two exchange functionals have been combined with the GGA for correlation of Perdew and Wang (PW91).[28] Additional BP86 calculations of the dipolar hyperfine coupling constants have been carried out with a modified version of the deMon-EPR code,[29,30] in which we have implemented a routine for the analysis of orbital contributions to A_{dip}.

The same vanadium orbital basis set has been used as in the g tensor calculations (see above), in combination with the 6-31G(d) basis set for the ligands. The default integration grids (int = fine grid option[23]) of the Gaussian 98 program and tight SCF convergence criteria (10^{-7} in RMS DM and 10^{-5} in MAX DM) have been applied.

Relationship between Spin-Hamiltonian Parameters and Electronic Structure. One of the aims of this study is to relate the spin Hamiltonian parameters obtained from theory/experiment to the electronic and molecular structure of a given paramagnetic center. This can be done along the lines of the classical second-order perturbation theory (PT) approach of Abragam and Pryce,[31] as further discussed by McGarvey,[15] by Abragam and Bleaney,[12] and by Mabbs and Collison.[16] This approach also enables us to provide a rough semiempirical estimate of spin−orbit (SO) contributions to the hyperfine coupling which are not explicitly accounted for in our present DFT calculations of hyperfine tensors.

Within the approach of Mabbs and Collison, the components of the Δg tensor and of the metal hyperfine tensor are given by[16]

$$\Delta g_{ij} = -2\xi_{n,l}\Lambda_{ij} \quad (6)$$

$$A_{ij} = P[-\kappa\delta_{ij} - 3cl_{ij} - 2\xi_{n,l}\Lambda_{ij} + 3c\xi_{n,l}\Lambda'_{ij}] \quad (7)$$

Here $P = g_e g_N \beta_e \beta_N \langle\varphi_o|r^{-3}|\varphi_o\rangle$ (φ_o is the singly occupied molecular orbital, SOMO),[32] $c = 2/[(2l-1)(2l+3)]$ (2/21 for a *d* electron), and $l_{ij} = \langle\varphi_o|\hat{l}_i\hat{l}_j + \hat{l}_j\hat{l}_i|\varphi_o\rangle - (1/3)l(l+1)\delta_{ij}$. The $-\kappa\delta_{ij}$ term accounts for the Fermi contact contribution to the isotropic part of the tensor, whereas the $-3cPl_{ij}$ term represents the first-order (SOMO) contribution to the anisotropic part of the tensor. $\xi_{n,l}$ is the spin−orbit coupling constant. The terms Λ_{ij} and Λ'_{ij} are defined as

$$\Lambda_{ij} = \sum_m \frac{\langle\varphi_o|\hat{l}_i|\varphi_m\rangle\langle\varphi_m|\hat{l}_j|\varphi_o\rangle}{\epsilon_m - \epsilon_o} \quad (8)$$

$$\Lambda'_{ij} = -\frac{i}{2}\sum_{t,r}\epsilon_{itr}\sum_m \frac{\langle\varphi_o|\hat{l}_r|\varphi_m\rangle\langle\varphi_m|\hat{l}_j\hat{l}_t + \hat{l}_t\hat{l}_j|\varphi_o\rangle}{\epsilon_m - \epsilon_o} \quad (9)$$

In the latter expression, ϵ_{itr} is 1 (−1) if (i,t,r) is an even (odd) permutation of (x,y,z) and 0 otherwise. The summation over m runs over all virtual *d*-type orbitals (cf. below). In expression

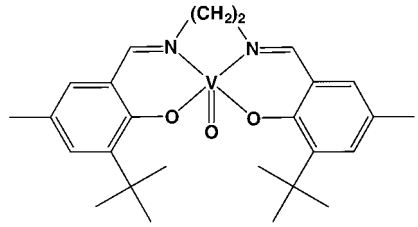

complex VOL[1]

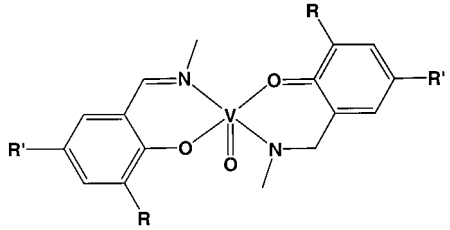

complex	R	R'
$VO(L^2)_2$	H	H
$VO(L^3)_2$	t-Bu	Me

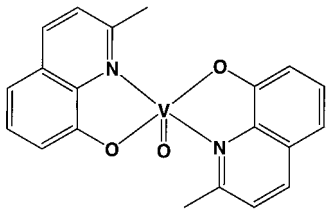

complex $VO\_(L^4)_2$

Figure 1. Vanadyl complexes studied. (a) VOL^1. (b) $VO(L^2)_2$ (R═H, R′═H) and $VO(L^3)_2$ (R═t-Bu, R′═Me). (c) $VO(L^4)_2$.

6 for the Δg tensor, Λ_{ij} approximates the paramagnetic part of Δg, given by eq 3. In the *A*-tensor expression 7, the Λ_{ij} elements account for the cross-terms between orbital Zeeman and spin dipolar operator;[33] the elements Λ'_{ij} represent second-order spin-dipolar contributions. One-third of the trace of T_{ij} gives the second-order "pseudocontact" contribution (A_{PC}) to the isotropic coupling.[34]

Equations 6 and 7 are often used either to determine MO compositions from the known spin Hamiltonian parameters or vice versa. The elements l_{ij}, Λ_{ij}, and Λ'_{ij} are expressed in terms of compositions and relative energies of the SOMO, φ_o, and of those virtual MOs, φ_m, which are dominated by metal d-orbital contributions (cf. ref 16, Chapter 9). The values of $\epsilon_m - \epsilon_o$ and of $\xi_{n,l}$ are usually estimated experimentally. Beyond interpretation purposes, this approach will in the following be used to estimate SO effects on the hyperfine tensor for the $VO(L^2)_2$ complex. The latter system is a d^1 complex possessing C_2 symmetry. The detailed expressions for the spin Hamiltonian parameters in this point group can be found on pp 384−386 of ref 16 (the reference appears to contain two typing errors[35]). The coefficients of the metal d orbitals in MOs $\varphi_o\varphi_1 \cdots \varphi_5$[36] have been determined from a restricted open-shell BP86 calculation. Each coefficient has been taken as the square root of the Mulliken gross orbital population summed over all basis functions of a given symmetry.[37] The value of the parameter *P* has been determined from the same calculation, using the fact that, within the first-order approximation, $T_{ZZ} = -3cPl_{zz}$. The relative energies, as well the *g* tensor components, cf. eqs 9.248−9.252 in ref 16, have been taken from experiment (ref 5). The value of the SO coupling constant (148.4 cm^{-1}) has been taken from ref 11.

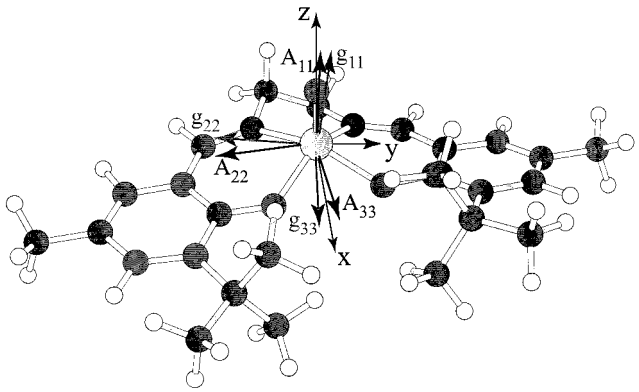

Figure 2. Standard orientation of the coordinate system, and the calculated *g* and *A* tensor for VOL^1.

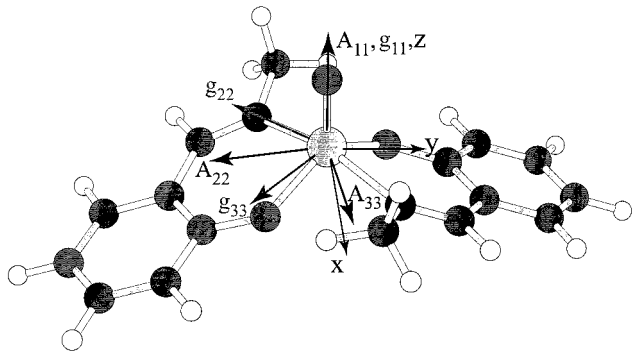

Figure 3. Standard orientation of the coordinate system, and the calculated *g* and *A* tensor for $VO(L^2)_2$.

Structures. Figure 1 shows the complexes studied: [*N*,*N*′-ethylenebis(*o*-*tert*-butyl-*p*-methylsalicylaldiminato)]oxovanadium(IV)═VOL^1(τ=0.26), bis(*N*-methylsalicylaldiminato)]-oxovanadium(IV) = $VO(L^2)_2$ (τ = 0.55), bis(*N*-methyl-*o*-(*tert*-butyl-*p*-methylsalicylaldiminato)oxovanadium(IV) = $VO(L^3)_2$ (τ = 0.70), and bis(2-methylquinoline-8-olate)oxovanadium-(IV) = $VO(L^4)_2$.

For VOL^1, $VO(L^2)_2$, and $VO(L^3)_2$, structural data from X-ray diffraction have been used.[5] Of these complexes, only $VO(L^2)_2$ has crystallographically imposed symmetry (C_2). No experimental structural data have been available for $VO(L^4)_2$. We have therefore optimized the structure in unrestricted Kohn−Sham calculations with the B3LYP functional (using the Gaussian 98 program[23]). The optimization employed a small-core effective-core potential (ECPs) and (8s7p6d)/[6s5p3d] GTO valence basis set for the metal,[38] ECPs with (4s4p1d)/[2s2p1d] basis sets[39] for the ligand atoms, and a (4s1p)/[2s1p] hydrogen basis.[40] The optimization has been performed within the C_2 symmetry indicated by the experiment.[11] The resulting structure parameters are reported as Supporting Information. The optimized $|VO_{axial}|$ bond length for $VO(L^4)_2$ (1.59 Å) is (within 0.01 Å) the same as found experimentally for VOL^1, $VO(L^2)_2$, $VO(L^3)_2$. The optimized $|VO_{ph}|$ bond length for $VO(L^4)_2$ (1.94 Å) lies also within the range of bond lengths found for the other complexes (1.89−1.94 Å). The optimized |VN| bond length for $VO(L^4)_2$ (2.16 Å) is somewhat longer than in the other complexes (2.06−2.10 Å). The distortion parameter τ for the optimized $VO(L^4)_2$ structure, 0.55, is the same as for $VO(L^2)_2$.

Orientation. All *g*- and *A*-tensor calculations have been performed for the following standard Cartesian coordinate system: The $\vec{VO}_{axial}$ vector defines the positive *z* direction. For VOL^1, the *y* axis lies in the $\overleftrightarrow{VO_{ph,1}O_{ph,2}}$ plane, perpendicular to the *z* axis.[41] For $VO(L^2)_2$, $VO(L^3)_2$, and $VO(L^4)_2$, the *y* axis

TABLE 1: Δg Tensors in Standard Axes System (in ppt)[a,b]

	Δg_{xx}	Δg_{yy}	Δg_{zz}	$\Delta g_{xy} = \Delta g_{yx}$	$\Delta g_{xz} = \Delta g_{zx}$	$\Delta g_{yz} = \Delta g_{zy}$
VOL[1]	−10.3	−12.4	−27.9	0.3	−3.2	1.7
$VO(L^2)_2$	−11.9	−13.0	−24.6	2.1	0.0	0.0
$VO(L^3)_2$	−10.1	−14.2	−25.6	2.7	0.7	−1.0
$VO(L^4)_2$	−10.0	−13.2	−29.8	2.0	0.0	0.0

[a] UDFT-VWN results with AMFI approximation for $\Delta g_{SO/OZ(2e)}$. [b] The actually computed g matrixes are slightly asymmetric. This information is not obtainable from the experiment. It means that the principal-axes system is not strictly an orthogonal one.[14] The values reported here and the principal values reported in Table 2 have been determined using the symmetrization procedure described in ref 14, p 91 (see also ref 17).

TABLE 2: Principal Δg Tensor Components (in ppt)[a]

	with $\Delta g_{SO/OZ(1e)}$ only				with $\Delta g_{SO/OZ(1e)} + \Delta g_{SO/OZ(2e)}$				experiment			
	Δg_{iso}	Δg_{11}	Δg_{22}	Δg_{33}	Δg_{iso}	Δg_{11}	Δg_{22}	Δg_{33}	Δg_{iso}	Δg_{11}	Δg_{22}	Δg_{33}
VOL[1]	−33.8	−58.2	−24.1	−19.1	−16.8	−28.6	−12.2	−9.7	−30	−49[b]	−21[b]	−19[b]
$VO(L^2)_2$	−32.7	−48.8	−29.1	−20.2	−16.5	−24.6	−14.5	−10.3	−30	−51[b]	−21[b]	−19[b]
$VO(L^3)_2$	−34.8	−55.6	−31.5	−17.4	−16.6	−25.7	−15.4	−8.8	−32	−55[b]	−23[b]	−18[b]
$VO(L^4)_2$	−35.2	−59.7	−28.3	−17.5	−17.7	−29.8	−14.2	−9.0	−29	−53[c]	−19[c]	−14[c]
									−30	−55(2)[d]	−21(2)[d]	−15(2)[d]

[a] UDFT-VWN results (cf. also ref 10). See also footnote *b* to Table 1. [b] Reference 5, estimated error of Δg is ±1 ppt, EPR on polycrystalline substance. [c] EPR on $[VO(mquin)_2]$ in a dilute crystal of $[GaCl(mquin)_2]$ (cf. ref 11). [d] Values obtained in pure crystal (cf. ref 11).

is defined in the same way but is additionally rotated by +45° around the $\vec{VO}_{axial}$ vector. This choice of the coordinate system, shown in Figures 2 and 3, is the same as used by Mabbs and Collison[16] for d^1 complexes possessing genuine or approximate C_2 or C_s symmetries.

3. Results and Discussion

Each of the complexes studied here contains one unpaired electron and may be regarded as a d^1 system. The SOMO is generally dominated by a metal $d_{x^2-y^2}$-type orbital (ca. 80%), and the largest ligand contribution corresponds to phenolate oxygen p orbitals (ca. 10%). The total spin population at vanadium reaches 1.10 because of the spin polarization of the $V{=}O_{axial}$ bond; a negative spin population of ca. −0.10 is left at the axial oxygen (all numbers refer to Mulliken population analyses of UBP86 results for the four complexes).

3.1. g-Tensor Calculations. Computed Δg components with respect to standard and principal axes are given in Tables 1 and 2, respectively. Both tables refer to the accurate atomic mean-field treatment of the $\Delta g_{SO/OZ(1e)}$ and $\Delta g_{SO/OZ(2e)}$ terms. In Table 2, we have also included results obtained if the $\Delta g_{SO/OZ(2e)}$ contributions are neglected. As found previously for a series of 3d complexes,[10] the latter results are in apparently better agreement with experiment than the former, obviously because of a compensation of errors due to the neglect of the $\Delta g_{SO/OZ(2e)}$ terms and errors in the DFT treatment. The proper inclusion of both one- and two-electron SO terms leads to a systematical underestimate of all components by ca. 40%. Gradient-corrected functionals also underestimate paramagnetic contributions to ^{57}Fe or ^{59}Co NMR chemical shifts by roughly the same relative amount, whereas hybrid functionals perform significantly better.[42] We are therefore presently implementing the calculation of g tensors with hybrid functionals. First tests suggest that this approach may indeed provide improved accuracy.[43]

After completion of this work, Carl et al. reported on their DFT calculations of A and g tensors of some vanadyl(IV) model complexes, with the aim of interpreting EPR spectra of VO^{2+} exchanged zeolites.[44] For their g tensor calculations, they used the two-component ZORA approach of van Lenthe et al.,[45] with the BP86 GGA functional. Carl et al. report significantly larger g shifts than in the present study and conclude that the DFT approach used provides excellent agreement with experiment. Unfortunately, this good performance is fortuitous and is probably due to cancellation of DFT errors with errors resulting from the neglect of spin polarization[46] (and partly from the incomplete treatment of the $\Delta g_{SO/OZ(2e)}$ terms[10]) in the two-component ZORA approach used.

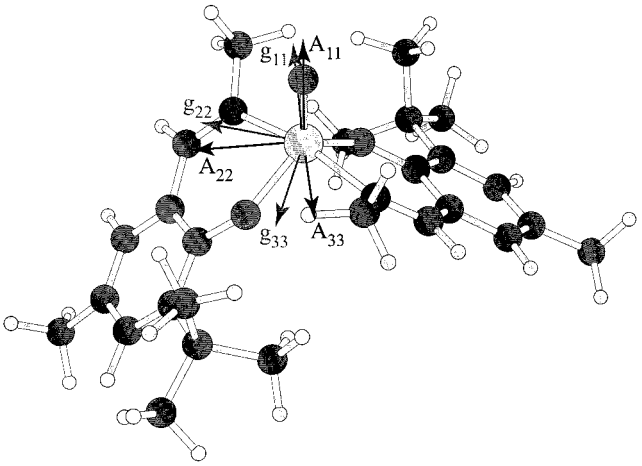

Figure 4. Orientation of the calculated g and A tensor for $VO(L^3)_2$.

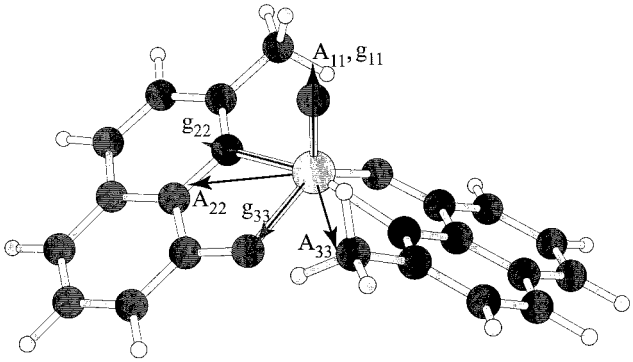

Figure 5. Orientation of the calculated g and A tensor for $VO(L^4)_2$.

The orientations of the g tensors are displayed in Figures 2−5. Table 3 includes the angles between the principal axes of the g tensor and the standard axes. The full specification of principals relative to standard axes is provided as Supporting Information. Table 3 shows that, for complexes with a trans arrangement of the phenolate oxygen atoms, the g_1 principal axis is either parallel or almost parallel to the z axis, whereas g_2 and g_3 are

TABLE 3: Rotation Angles (in Degrees) between Principal Axes of *g* and *A* Tensors and the Standard Axes[a]

complex	$\angle(g_1,z)$	$\angle(a_1,z)$	$\angle(g_1,a_1)$	$\angle(g_2,y)$	$\angle(a_2,y)$	$\angle(g_2,a_2)$	$\angle(g_3,x)$	$\angle(a_3,x)$	$\angle(g_3,a_3)$
VOL^1	11.6	4.7	6.9	6.1	11.5	11.1	10.0	12.4	12.0
$VO(L^2)_2$	0.0	0.0	0.0	37.7	11.3	49.0	37.7	11.3	49.0
$VO(L^3)_2$	6.6	0.8	6.2	26.9	5.1	31.9	26.2	5.2	31.4
$VO(L^4)_2$	0.0	0.0	0.0	25.8	10.0	35.7	25.8	10.0	35.7

[a] UDFT-VWN results with AMFI approximation for $\Delta g_{SO/OZ(2e)}$ (*g* tensor) and UBHPW91 results (*A* tensor). See also footnotes to Table 1.

rotated with respect to *y* and *x*, on average by 30°. For VOL^1, g_2 is almost parallel to the *y* axis, whereas g_1 and g_3 are rotated with respect to *z* and *x* by 12° and 10°, respectively (note that neglect of the $\Delta g_{SO/OZ(2e)}$ terms affects the tensor orientation negligibly). For these three systems, there is no experimental information to be compared with regarding the orientation of the *g* tensor with respect to the molecular framework. We focus therefore on the interpretation of the computational results. We will base our discussion on the perturbational approach discussed in section 2.

We are dealing here with d^1 complexes possessing genuine C_2 symmetry ($VO(L^2)_2$ and $VO(L^4)_2$), approximate C_2 symmetry ($VO(L^3)_2$), or approximate C_s symmetry (VOL^1). As a consequence, for $VO(L^2)_2$ and $VO(L^4)_2$, one of the principal axes (g_1) must coincide with the 2-fold axis (*z*) for symmetry reasons.[14] In a hypothetical VOL^1 molecule possessing genuine C_s symmetry, one of the principal axes would have to be perpendicular to the *xz* symmetry plane and thus coincident with the *y* axis. The actual deviation of g_2 from *y* (6°, cf. Table 3) may thus be considered to be a measure of the distortion from C_s symmetry. For $VO(L^3)_2$, by analogy, the deviation of g_1 from *z* (7°) corresponds to the distortion from C_2 symmetry.

The extent of the rotation of the principal axes relative to the standard axes depends on the values of the off-diagonal tensor elements[16] but also on the relative sizes of the principal components. For genuinely C_2 symmetrical complexes, it can be shown that the angle φ between g_2 and *y* and between g_3 and *x* is related to the off-diagonal matrix g_{xy} element and the principal g_{22} and g_{33} components via

$$2g_{xy} = (g_{22} - g_{33}) \sin 2\varphi \qquad (10)$$

The g_{xy} component is of the same size (cf. Table 1) for $VO(L^2)_2$ and $VO(L^4)_2$, but the value of $|g_{22} - g_{33}|$ is smaller for the former complex (cf. Table 2). Consequently, g_2 and g_3 deviate more from the *y* and *x* directions, respectively, for $VO(L^2)_2$ than for $VO(L^4)_2$ (cf. Table 3).

According to Mabbs and Collison,[16] the rotation of g_2 and g_3 relative to *y* and *x* is dominated by the magnitude of the $d_{x^2-y^2} \rightarrow d_{xz}$ and $d_{x^2-y^2} \rightarrow d_{yz}$ contributions (cf. eqs 9.233−9.237 in ref 16), which determine the magnitudes of the g_{xx}, g_{yy}, and g_{xy} elements. By analogy, the rotation of g_1 and g_3 with respect to *z* and *x* for VOL^1 is determined mainly by the $d_{x^2-y^2} \rightarrow d_{xy}$ and $d_{x^2-y^2} \rightarrow d_{yz}$ contributions (cf. eqs 9.243 and 9.247 in ref 16).[47] An analysis of different contributions to the calculated *g* shifts shows that the paramagnetic (one-electron and two-electron SO) contributions represent 99% of the *g* tensor components given in Tables 1 and 2. An analysis of the orbital contributions to *g* tensor elements further reveals that the SO terms corresponding to the excitations from the SOMO greatly dominate the *g* tensor elements. Thus, our results show that the approach of Mabbs and Collison, which emphasizes the SOMO contributions, provides reasonable insight into the origin of the *g* tensor.

3.2. *A*-Tensor Calculations. Our density-functional results for the hyperfine tensor of vanadium with respect to standard and principal axes are given in Tables 4 and 5, respectively.

TABLE 4: *A* Tensors in the Standard Axes (in MHz)[a]

	A_{xx}	A_{yy}	A_{zz}	$A_{xy} = A_{yx}$	$A_{xz} = A_{zx}$	$A_{yz} = A_{zy}$
VOL^1	107.6	98.0	−205.6	−1.7	−24.8	−1.7
$VO(L^2)_2$	112.4	93.5	−205.9	−3.9	0.0	−3.9
$VO(L^3)_2$	119.3	83.7	−202.9	−3.2	1.8	−3.2
$VO(L^4)_2$	114.7	90.9	−205.6	−4.3	0.0	−4.3

[a] UBHPW91 results.

Part of the information in Table 5 is graphically displayed in Figures 6−8.[48] The SOMO provides a small direct contribution to the isotropic hyperfine coupling constants (HFCCs), because of a slight mixing-in of the metal 4s orbital. Nevertheless, overall A_{iso} is dominated by spin polarization and is thus negative. The anisotropic tensor reflects the composition of the SOMO, having one negative component along the *z* axis and two positive components within the *xy* plane,[49] pointing between the V−N and $V-O_{phenolate}$ bonds. Like the *g* tensor, the *A* tensor deviates from axial symmetry.[50] The smaller of the positive components points into the direction of the chelate ligands, and the larger one points out of the complex.

At the nonrelativistic (first-order) level of theory, the BHPW91 functional provides the best agreement with experiment for both the isotropic and the anisotropic parts of the hyperfine tensor. As has been stressed in our recent study,[8] GGA functionals typically underestimate the spin polarization of s-type metal core orbitals. The latter is enhanced by exact-exchange mixing into υ_x, frequently leading to improved agreement with experimental A_{iso} data with hybrid functionals (provided that spin contamination remains low). Figure 6 illustrates the enhancement of spin polarization by inclusion of exact exchange for three of the vanadyl complexes. It also shows that, for systems with related electronic structures, the deficiencies of the state-of-the-art density functionals are systematic. An underestimate of core−shell spin polarization with the BP86 GGA functional is also apparent from the results of the very recent *A*-tensor calculations of Carl et al.[44] for a series of vanadyl model complexes.

Similarly, adequate spin polarization of metal p-type core orbitals is required to reproduce the hyperfine tensor anisotropy.[8,9,51] The absolute values of the dipolar tensor components are quantitatively reproduced only with the BHPW91 functional (cf. Table 5 and Figure 7). B3PW91, and particularly BP86, underestimate all anisotropic components. On the other hand, all unrestricted DFT approaches applied describe the rhombicity of the hyperfine tensor well. The $(T_{33} - T_{22})$ difference does not suffer from the systematic underestimate of spin polarization, as it is determined mainly by the composition of the singly occupied molecular orbital. The relative magnitudes of spin polarization of the metal $2p_x$, $3p_x$ and $2p_y$, $3p_y$ orbitals correspond to the rhombicity of the SOMO contribution to the anisotropic HFC tensor. Thus, although the absolute values of the T_{22} and T_{33} components are significantly affected by the spin-polarization contributions, the asymmetry of the tensor $(T_{33} - T_{22})$ is reduced only slightly by core−shell spin polarization.

The present DFT calculations do not include relativistic corrections, which may be quite important for systems with

TABLE 5: Principal *A* Tensor Components (in MHz)[a]

	BP86	B3PW91	BHPW91	exp./nominal $\langle S^2 \rangle$
		VOL^1		
A_{iso}	−183.0	−231.7	−299.6	−274.3
T_{11}, T_{22}, T_{33}	−177.9, 79.0, 98.9	−193.9, 89.5, 104.4	−207.8, 97.8, 110.0	−209.3, 96.8, 112.4
$\langle S^2 \rangle^b$	0.7566	0.7618	0.7754	0.7500
		$VO(L^2)_2$		
A_{iso}	−179.0	−230.1	−297.8	−273.9
T_{11}, T_{22}, T_{33}	−182.2, 79.6, 102.7	−194.3, 86.5, 107.8	−205.9, 92.7, 113.2	−208.8, 94.0, 114.7
$\langle S^2 \rangle^b$	0.7578	0.7661	0.7856	0.7500
		$VO(L^3)_2$		
A_{iso}	−157.6	−217.0	−290.4	−264.3
T_{11}, T_{22}, T_{33}	−172.9, 63.8, 109.1	−189.5, 74.1, 115.4	−203.0, 83.4, 119.6	−207.3, 86.2, 121.0
$\langle S^2 \rangle^b$	0.7586	0.7655	0.7838	0.7500
		$VO(L^4)_2$		
A_{iso}	−164.3	−216.8	−295.8	−262.9
T_{11}, T_{22}, T_{33}	−183.0, 76.7, 106.3	−194.3, 82.7, 111.7	−205.6, 90.2, 115.5	−208.7, 93.2, 115.4
$\langle S^2 \rangle^b$	0.7580	0.7645	0.7834	0.7500

[a] Unrestricted Kohn−Sham calculations with specified exchange-correlation functionals. [b] These $\langle S^2 \rangle$ values pertain to the Kohn−Sham wave function, i.e., to the noninteracting reference system rather than to the real system. Such data are nevertheless expected to give a reasonable and useful representation for the real system as well (see, e.g., Baker, J.; Scheiner, A.; Andzelm, J. *Chem. Phys. Lett.* **1993**, *216*, 380).

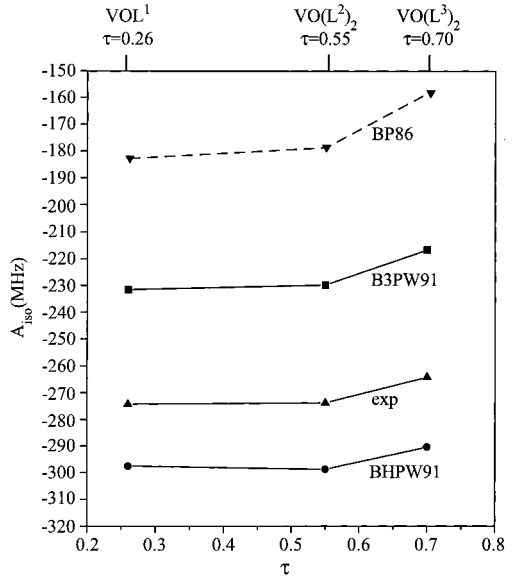

Figure 6. Dependence of the isotropic hyperfine coupling constants on the distortion parameter τ. BP86, B3PW91, BHPW91, and experimental results are compared for VOL^1, $VO(L^2)_2$, and $VO(L^3)_2$.

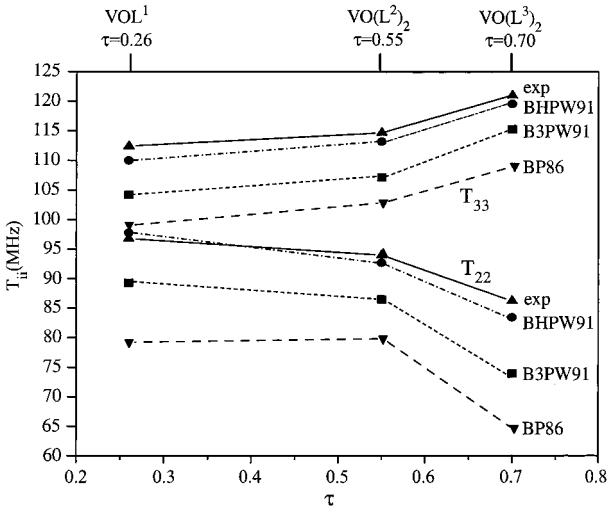

Figure 7. Dependence of the anisotropic hyperfine tensor components on the distortion parameter τ. BP86, B3PW91, BHPW91, and experimental results are compared.

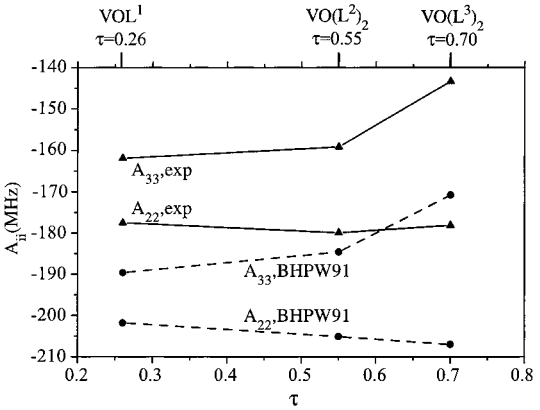

Figure 8. Dependence of the total (isotropic + anisotropic) hyperfine tensor components on the distortion parameter τ. BHPW91 and experimental results are compared.

significant *g* tensor anisotropy. To obtain a simple semiempirical estimate of SO corrections, as well as an improved interpretation of the HFC anisotropy, we have used the PT approach described in section 2 to express the *A* tensor of $VO(L^2)_2$. The first-order (SOMO) contributions to the anisotropic part of the *A* tensor have been estimated as −192.8 (T_{zz}), 80.3 (T_{xx}), 112.5 (T_{yy}), and 1.4 ($T_{xy} = T_{yx}$) MHz. The second-order Λ_{ij} elements provide an additional −17.9 (T_{zz}), −6.7 (T_{xx}), and −7.4 (T_{yy}) MHz.[52] Finally, the Λ'_{ij} elements have been estimated as −3.4 (T_{zz}), −0.6 (T_{xx}), −1.0 (T_{yy}), −0.1 (T_{xy}), and 0.2 (T_{yx}) MHz. After summing these contributions and transforming the resulting tensor to its principal axes, we obtain the following components: −214.1 (T_{11}), 75.1 (T_{22}), and 102.1 (T_{33}) MHz. This tensor has a nonzero trace that, multiplied by a factor of $^1/_3$, gives the pseudocontact contribution to the isotropic HFCC (−12.3 MHz). Subtracting the pseudocontact term from the T_{ii} components, we obtain a traceless anisotropic HFC tensor in the second-order approximation. The components of this tensor are −201.8, 87.4, and 114.4 MHz, of which the second-order contributions represent −9.0, 4.6, and 4.4 MHz, respectively. After subtraction of these contributions from the experimental HFC tensor, the B3PW91 and BHPW91 functionals would appear to describe the first-order hyperfine coupling about equally well. The former underestimates and the latter overestimates A_{iso} and all T_{ii} components.

Besides an estimate of the SO contributions, the perturbation theoretical approach *qualitatively* reproduces and rationalizes the rhombicity of the *A* tensor. As discussed above, the difference $T_{22} - T_{33}$ arises mainly from the first-order (SOMO) contribution. The only first-order term which can account for this is a very small (0.2%) symmetry-allowed mixing of the metal d_{z^2} orbital into the SOMO, cf. eqs 9.239−9.242 in ref 16.[53] This mixing hybridizes the unpaired electron density outside of the chelate rings (i.e., in the *x* direction, cf. Figures 2 and 3), so that $T_{22} < T_{33}$. This approximate treatment cannot aim at *quantitative* agreement with the experiment. The rhombicity of the tensor ($T_{22} - T_{33}$) is overestimated. This is understandable, as explicit restricted (ROBP86) Kohn−Sham calculations, using formula 5, also overestimate T_{ii} ($T_{11} = -192.8$ MHz, $T_{22} = 80.3$ MHz, and $T_{33} = 112.5$ MHz). The influence of the second-order contributions on the asymmetry of the hyperfine tensor is only minor ($T_{33} - T_{22}$ is decreased by 0.2 MHz), as both Λ_{ij} and the Λ'_{ij} contributions to T_{33} and T_{22} have identical sign and similar magnitudes. The rhombicity of the HFC tensor in $VO(L^4)_2$ can be understood along the same lines as that for $VO(L^2)_2$. The situation is more complicated for $VO(L^1)$ and $VO(L^3)_2$, because of the lack of symmetry.

An interesting observation has been made by Cornman et al. on the correlation of $A_{33} - A_{22}$ (in their notation $A_{xx} - A_{yy}$) and the distortion parameter τ for $VO(L^1)$, $VO(L^2)_2$, and $VO(L^3)_2$.[5] Although one of the components was found to be relatively stable with respect to the distortion, the other experienced significant enhancement (cf. Figure 8). Our calculations allow an unambiguous breakdown of the experimental tensor into its isotropic and dipolar parts. Although T_{33} and A_{iso} increase with increasing τ (A_{iso} becomes less negative; cf. Figure 6), T_{22} decreases by approximately the same magnitude (cf. Figure 7). Because of the combination of these effects, A_{22} remains constant, whereas A_{33} changes significantly along the SQP-5 → TBP-5 distortion coordinate (Figure 8). Thus, in contrast to the interpretation in ref 5, increasing τ affects both in-plane dipolar contributions to a similar extent. The increased difference between T_{22} and T_{33} from $VO(L^2)_2$ to $VO(L^3)_2$ may be understood in terms of SOMO composition: (i) The metal d_{xz} and d_{yz} orbitals mix into the SOMO with different coefficients for $VO(L^3)_2$ but not for $VO(L^2)_2$, where this is prohibited by symmetry. (ii) The vanadium d_{z^2} orbital mixes into the SOMO more for $VO(L^3)_2$ than for $VO(L^2)_2$. Both contributions hybridize the spin density further out of the chelate rings in $VO(L^3)_2$. In $VO(L^1)_2$, the metal d_{xz} and d_{yz} orbitals mix less into the SOMO than in $VO(L^3)_2$, and their contribution to the anisotropy in T_{22} and T_{33} is compensated by reduced d_{z^2} mixing, resulting in a total anisotropy that is similar to that in $VO(L^1)$.

A comparison of the *A*-tensor results for $VO(L^2)_2$ and $VO(L^4)_2$ (cf. Table 5) reveals that the anisotropic HFC tensor components of both complexes are very close, in agreement with identical distortion parameters τ (0.55) and similar d_{xy}, $d_{x^2-y^2}$, and d_{z^2} contributions to the SOMO. Because of a higher 4s orbital contribution to the SOMO for $VO(L^4)_2$, the isotropic HFCC is less negative than for $VO(L^2)_2$.

The orientations of the *A* tensors are shown in Figures 2−5, together with those of the *g* tensors. Table 3 includes the angles between the principal axes of the *A* and *g* tensors and the standard axes. The full specification of the principal axes of the *A* tensor with respect to the standard axes is given as Supporting Information. Table 3 shows that a_1 is oriented either parallel or close to parallel to the *z* axis (rotated from *z* by maximally 6°). The axes of a_2 and a_3 are rotated with respect to *y* and *x* by maximally 12°. This is much less than for the *g*-tensor axes, because the off-diagonal elements of the *A* tensor are much smaller with respect to the asymmetry in the principal components than those for the *g* tensor (cf. eq 10; Tables 4 and 1). Generally, the hyperfine tensor is controlled by the nature of the ground-state wave function. In contrast, the *g* tensor reflects also energies and character of the excited states.[16] These appear to be particularly sensitive to the local metal coordination. For the same reason, the SQP-5 → TBP-5 distortion influences the *A* tensor orientation relatively little, whereas the *g* tensor is reoriented significantly.

Only for $VO(L^4)_2$, experimental information is available on the relative orientation of *g* and *A* tensors.[11] Single-crystal data indicate that the *g*-tensor component with the smallest *g* shift (in our notation g_{33}) is rotated by 27.5° relative to the *A*-tensor component with the smallest magnitude of the dipolar interaction (in our notation A_{22}): $\angle(a_2,g_3) = 27.5°$. Our computational results suggest that the A_{22} orientation is closer to the g_{22} orientation than to the g_{33} orientation: $\angle(a_2,g_2) = 35.7°$ and $\angle(a_2,g_3) = 54.3°$ (cf. Table 3). It is possible that deficiencies in our DFT treatment are responsible for the different rotation angles. However, the angle is affected significantly neither by the inclusion or neglect of the $\Delta g_{SO/OZ(2e)}$ operators nor by the use of local or gradient-corrected density functionals. At the moment, we can only state that theory agrees with experiment on a ca. 30° relative rotation of the "perpendicular" principal components of *g* and *A* tensors. Further theoretical and/or experimental work is needed to decide which *g*- and *A*-tensor components (a_2, a_3, g_2, and g_3) have the most similar orientations.

4. Conclusions

The increasing rhombicity of both *A* and *g* tensors with increasing deviations of the structures of vanadyl(IV) complexes from a regular square-pyramidal (SQP-5) coordination arrangement is reproduced by our density functional calculations. We could therefore provide improved interpretations of the observed trends in terms of the SOMO compositions and of spin−orbit coupling. In addition to the magnitudes of the principal components of both tensors, the calculations provide also their orientations relative to each other and relative to the molecular framework. Such information is more difficult to obtain experimentally. In the present series of systems, the necessary single-crystal experiments were only available for one of the systems, $VO(L^4)_2$. Although some discrepancies remain in the designation of the components in this case, all calculations indicate clearly that the *g* tensor is affected more by the structural distortions of the SQP-5 arrangement than the metal *A* tensor. This may be rationalized by the fact that to first order the hyperfine tensor depends only on the spin-density distribution of the ground state, whereas the *g* tensor is a response property and thus also reflects the compositions of excited states. As a consequence, the *A* and *g* tensors are noncoaxial in all of the systems studied here. The orientation of *A* and particularly of *g* tensors with respect to the molecular framework, or the experimentally more accessible relative orientations of *g* and *A* tensors, may be very sensitive probes of the local symmetry and coordination of the oxovanadium group. In the case of the *A* tensor, the increasing rhombicity with increasing SQP-5 → TBP-5 distortion arises because of the mixing of metal d_{z^2} orbitals (made possible by the transformation from SQP-5 toward TBP-5 coordination) but also of metal d_{xz} and d_{yz} orbitals (allowed by the deviation from C_2 symmetry), into the $d_{x^2-y^2}$-type SOMO.

Apart from interpretational purposes, the present study has also served as a further validation of DFT approaches for the

calculation of EPR parameters in transition metal complexes. The vanadyl complexes studied here exhibit a SOMO with relatively little overlap to doubly occupied metal valence orbitals. In agreement with our previous considerations,[8,9] spin contamination with increasing exact-exchange mixing is therefore not a serious problem. Hybrid functionals (B3PW91 and BHPW91) provide better agreement with experimental isotropic HFCCs than a GGA functional (BP86), because of an improved description of the spin polarization of metal s-type core shells.[8] All functionals, including the BP86 GGA, reproduce well the experimentally observed trends in the anisotropy of the *A* tensor with increasing structural distortion (which is dominated by the SOMO composition; cf. above).

As found already in the previous extensive validation of our DFT approach for the calculation of electronic *g* tensors,[10] LDA or GGA functionals underestimate the paramagnetic ($\Delta g_{SO/OZ}$) contributions systematically by ca. 40% for 3d transition metal complexes (whereas a slight overestimate by ca. 10% is typical for main group radicals). In agreement with the suggestions of Patchkowskii and Ziegler,[54] we attribute this to deficiencies of the GGA/LDA functionals in describing both energy denominators and matrix elements in the second-order perturbation theory expressions (cf. eq 3). Although a partial or complete neglect of the $\Delta g_{SO/OZ(2e)}$ terms improves the agreement with experiment in the 3d complexes, this is certainly no satisfactory approach from a theoretical point of view. First tests suggest that hybrid functionals may provide better accuracy (cf. section 3.1[43]).

Acknowledgment. We thank Drs. Pavel Kubáček, Dominik Munzar (Brno), and Juha Vaara (Helsinki) for helpful discussions. Drs. Olga L. Malkina (Bratislava) and Reinaldo Pis-Diez (UNLP, Argentina) kindly provided us with codes that simplified the analyses carried out. This work has been supported by Deutsche Forschungsgemeinschaft (Schwerpunktprogramm "Hochfeld-EPR", SPP1051) and by Fonds der chemischen Industrie. Further support came from the graduate college "Moderne Methoden der Magnetischen Resonanz" at Universität Stuttgart.

Supporting Information Available: The DFT-optimized cartesian coordinates of bis(2-methylquinoline-8-olate)oxovandium(IV) (Table 1), as well as principal axes of *g* tensors (Table 2) and hyperfine tensors (Table 3). This material is available free of charge via the Internet at http://pubs.acs.org.

References and Notes

(1) (a) Vilter, H. In *Metal Ions in Biological Systems*; Sigel, H., Sigel, A., Eds.; Marcel Dekker: New York, 1995; Vol. 31, pp 325−362. (b) Eady, R. R. In *Metal Ions in Biological Systems*; Sigel, H., Sigel, A., Eds.; Marcel Dekker: New York, 1995; Vol. 31, pp 363−405. (c) Butler, A.; Walker, J. V. *Chem. Rev.* **1993**, *93*, 1937−1944.

(2) See, e.g., (a) Shechter, Y.; Karlish, S. J. D. *Nature* **1980**, *284*, 556−558. (b) Shechter, Y.; Meyerovitch, J.; Farfel, Z.; Sack, J.; Bruck, R.; Bar-Meir, S.; Amir, S.; Degani, H.; Karlish, S. J. D. In *Vanadium in Biological Systems*; Chasteen, N. D., Ed.; Kluwer Academic Publishers: Dordrecht, The Nederlands, 1990; pp 129−142. (c) Orvig, C.; Thompson, K. H.; Battel, M.; McNeal, J. H. In *Metal Ions in Biological Systems*; Sigel, H., Sigel, A., Eds.; Marcel Dekker: New York, 1995; Vol. 31, pp 575−594.

(3) Crans, D. C. *Comments Inorg. Chem.* **1994**, *16*, 35−76.

(4) Morky, L. M.; Carrano, C. J. *Inorg. Chem.* **1993**, *32*, 6119−6121.

(5) Cornman, C. R.; Geiser-Bush, K. M.; Rowley, S. P.; Boyle, P. D. *Inorg. Chem.* **1997**, *36*, 6401−6408.

(6) Grant, C. V.; Geiser-Bush, K. M.; Cornman, C. R.; Britt, R. D. *Inorg. Chem.* **1999**, *38*, 6285−6288.

(7) Grant, C. V.; Cope, W.; Ball, J. A.; Maresch, G. G.; Gaffney, B. J.; Fink, W.; Britt, R. D. *J. Phys. Chem. B* **1999**, *103*, 10627−10631.

(8) Munzarová, M.; Kaupp, M. *J. Phys. Chem. A* **1999**, *103*, 9966.

(9) Munzarová, M. L.; Kubáček, P.; Kaupp, M. *J. Am. Chem. Soc.* **2000**, *122*, 11900−11913.

(10) Malkina, O. L.; Vaara, J.; Schimmelpfennig, B.; Munzarová, M.; Malkin, V. G.; Kaupp, M. *J. Am. Chem. Soc.* **2000**, *122*, 9206−9218.

(11) Collison, D.; Gahan, B.; Mabbs, F. *J. Chem. Soc., Dalton Trans.* **1987**, 111.

(12) Abragam, A.; Bleaney, B. *Electron Paramagnetic Resonance of Transition Ions*; Clarendon Press: Oxford, 1970.

(13) Atherton, N. M. *Principals of Electron Spin Resonance*; Prentice Hall: New York, 1993.

(14) Weil, J. A.; Bolton, J. R.; Wertz, J. E. *Electron Paramagnetic Resonance: Elementary Theory and Practical Applications*; Willey & Sons: New York, 1994.

(15) McGarvey, B. R. In *Transition Metal Chemistry: A Series of Advances*; Carlin, R. L., Ed.; Marcel Dekker: New York, 1966; Vol. 3, pp 89−201.

(16) Mabbs, F. E.; Collison, D. *Electron Paramagnetic Resonance of d Transition Metal Compounds*; Elsevier: Amsterdam, The Netherlands, 1992.

(17) Harriman, J. E. *Theoretical Foundations of Electron Spin Resonance*; Academic Press: New York, 1978.

(18) Schreckenbach, G.; Ziegler, T. *J. Phys. Chem. A* **1997**, *101*, 3388.

(19) Hess, B. A.; Marian, C. M.; Wahlgren, U.; Gropen, O. *Chem. Phys. Lett.* **1996**, *251*, 365.

(20) The code used is from the following: Schimmelpfennig, B. *AMFI, Atomic Spin−Orbit Mean-Field Integral Program*; Stockholms Universitet: Stockholm, Sweden 1996.

(21) Vosko, S. H.; Wilk, L.; Nusair, M. *Can. J. Chem.* **1980**, *58*, 1200.

(22) Godbout, N.; Salahub, D. R.; Andzelm, J.; Wimmer, E. *Can. J. Chem.* **1992**, *70*, 560.

(23) Frisch, M. J.; Trucks, G. W.; Schlegel, H. B.; Scuseria, G. E.; Robb, M. A.; Cheeseman, J. R.; Zakrzewski, V. G.; Montgomery, J. A., Jr.; Stratmann, R. E.; Burant, J. C.; Dapprich, S.; Millam, J. M.; Daniels, A. D.; Kudin, K. N.; Strain, M. C.; Farkas, O.; Tomasi, J.; Barone, V.; Cossi, M.; Cammi, R.; Mennucci, B.; Pomelli, C.; Adamo, C.; Clifford, S.; Ochterski, J.; Petersson, G. A.; Ayala, P. Y.; Cui, Q.; Morokuma, K.; Malick, D. K.; Rabuck, A. D.; Raghavachari, K.; Foresman, J. B.; Cioslowski, J.; Ortiz, J. V.; Stefanov, B. B.; Liu, G.; Liashenko, A.; Piskorz, P.; Komaromi, I.; Gomperts, R.; Martin, R. L.; Fox, D. J.; Keith, T.; Al-Laham, M. A.; Peng, C. Y.; Nanayakkara, A.; Gonzalez, C.; Challacombe, M.; Gill, P. M. W.; Johnson, B. G.; Chen, W.; Wong, M. W.; Andres, J. L.; Head-Gordon, M.; Replogle, E. S.; Pople, J. A. *Gaussian 98*, revision A.7; Gaussian, Inc.: Pittsburgh, PA, 1998.

(24) Becke, A. D. *Phys. Rev. A* **1988**, *38*, 3098.

(25) Perdew, J. P.; Wang, Y. *Phys. Rev. B* **1986**, *33*, 8822; **1986**, *34*, 7406.

(26) Becke, A. D. *J. Chem. Phys.* **1993**, *98*, 5648.

(27) Becke, A. D. *J. Chem. Phys.* **1993**, *98*, 1372.

(28) (a) Perdew, J. P. *Physica B* **1992**, *172*, 1. (b) Perdew, J. P. In *Electronic Structure of Solids '91*; Ziesche, P., Eschring, H., Eds.; Akademie Verlag: Berlin, Germany, 1991. (c) Perdew, J. P.; Wang, Y. *Phys. Rev. B* **1992**, *45*, 13244.

(29) Malkin, V. G.; Malkina, O. L.; Eriksson, L. A.; Salahub, D. R. In *Modern Density Functional Theory: A Tool for Chemistry, Vol. 2 of Theoretical and Computational Chemistry*; Politzer, P., Seminario, J. M., Eds.; Elsevier: Amsterdam, The Netherlands, 1995; pp 273−347.

(30) (a) Salahub, D. R.; Fournier, R.; Mlynarski, P.; Papai, I.; St-Amant, A.; Ushio, J. In *Density Functional Methods in Chemistry*; Labanowski, J., Andzelm, J., Eds.; Springer: New York, 1991. (b) St-Amant, A.; Salahub, D. R. *Chem. Phys. Lett.* **1990**, *169*, 387.

(31) Abragam, A.; Pryce, M. H. L. *Proc. R. Soc. A* **1951**, *205*, 135.

(32) The parameter *P* depends on the radial wave function of the metal atom in the field of ligands and is usually treated as an adjustable parameter.

(33) At this level of theory, the elements of $2\xi_{n,l}\Lambda_{ij}$ correspond to the Δg_{ij} elements.

(34) Although the first-order contribution to T_{ij} is symmetrical and traceless, the Λ_{ij} contribution is symmetrical but not traceless. In general, Λ'_{ij} is neither symmetrical nor traceless. See ref 14 for a lucid discussion.

(35) According to our calculation, the correct formulas for coefficients C_7 and C_9 should read: $C_7 = -3e_3a_1 - 3f_3b_1 - (3)^{1/2}e_3c_1$; $C_9 = 3f_3a_1 - 3e_3b_1 - (3)^{1/2}f_3c_1$.

(36) Formulas 9.248−9.252 of ref 16 have been derived from (9) and (10), restricting the summation over *m* to the four MOs with the largest d-orbital contributions. In our calculations, we have therefore chosen the four unoccupied MOs with largest computed metal d character.

(37) For the standard orientation of the molecule, we obtained the following d-orbital mixings: ϕ_o (MO 45*a*) = $0.977d_{xy} + 0.098d_{x^2-y^2} - 0.040d_{z^2}$; ϕ_1 (47*a*) = $0.095d_{xy} - 0.420d_{x^2-y^2} + 0.387d_{z^2}$; ϕ_2 (44*b*) = $0.000d_{xz} + 0.764d_{yz}$; ϕ_3 (45*b*) = $0.721d_{xz} - 0.108d_{yz}$; ϕ_4 (49*a*) = $-0.082d_{xy} + 0.516d_{x^2-y^2} + 0.274d_{z^2}$.

(38) Dolg, M.; Wedig, U.; Stoll, H.; Preuss, H. *J. Chem. Phys.* **1987**, *86*, 866.

(39) (a) Bergner, A.; Dolg, M.; Küchle, W.; Stoll, H.; Preuss, H. *Mol. Phys.* **1993**, *80*, 1431. (b) d-type polarization functions have been taken from the following: *Gaussian Basis Sets for Molecular Calculations*; Huzinaga, S., Ed.; Elsevier: New York, 1984.

(40) Dunning, T. H.; Hay, H. In *Methods of Electronic Structure Theory, Vol. 3 of Modern Theoretical Chemistry*; Schaefer, H. F., III., Ed.; Plenum Press: New York, 1977.

(41) This definition is unique, unless the $\overleftrightarrow{VO_{ph,1}O_{ph,2}}$ plane is perpendicular to the VO_{axial} vector. This is not the case for any of the complexes studied here.

(42) (a) Bühl, M. *Chem. Phys. Lett*. **1997**, *267*, 251. (b) See, also: Godbout, N.; Oldfield, E. *J. Am. Chem. Soc.* **1997**, *119*, 8065.

(43) Kaupp, M.; Reviakine, R.; Malkina, O. L.; Arbuznikov, A.; Schimmelpfennig, B.; Malkin, V. G. *J. Comput. Chem.* In press.

(44) Carl, P. J.; Isley, S. L.; Larsen, S. C. *J. Phys. Chem. A* **2001**, *105*, 4563.

(45) van Lenthe, E.; Wormer, P. E. S.; van der Avoird, A. *J. Chem. Phys.* **1997**, *107*, 2488.

(46) See, e.g.: van Lenthe, E.; van der Avoird, A.; Hagen, W. R.; Reijerse, E. J. *J. Phys. Chem. A* **2000**, *104*, 2070, and references therein.

(47) Turning this line of reasoning around, from the theoretical orientations of the principal axes, one can estimate the relative sizes of the individual spin−orbit coupling terms.

(48) As Figures 6−8 serve as the interpretation of the experimental findings in ref 5, we have not included the data for $VO(L^4)_2$.

(49) This is rigorously true only for the two complexes possessing C_2 symmetry. For the two other complexes, we observe small deviations from the indicated directions, cf. below.

(50) For the definition of the asymmetry (rhombicity) parameter, cf. ref 14, p 116.

(51) Belanzoni, P.; Baerends, E. J.; van Asselt, S.; Langewen, P. B. *J. Phys. Chem*. **1995**, *99*, 13094.

(52) The corresponding contributions to $T_{x'y'}$ and $T_{y'x'}$ are zero, because of zero nondiagonal elements of the *g* tensor (cf. section 2).

(53) We note that the asymmetry of the HFC tensor can be influenced also by mixing of the metal 4s orbital into the SOMO, which is symmetry-allowed. This mixing is not considered in the usual interpretations, cf. refs 12, 15, and 16.

(54) Patchkovskii, S.; Ziegler T. *J. Chem. Phys.* **1999**, *111*, 5730.